Vibration System Analysis of Radial Magnetic Bearing for MMR Condition

Dokyu Kim [a], SeungJoon Baik [b], Jeong Ik Lee [a*]
[a]*Department of Nuclear and Quantum Engineering, KAIST, Daejeon, South Korea*
[b] *Korea Atomic Energy Research Institute, Daejeon, South Korea*
Corresponding author : jeongiklee@kaist.ac.kr

1. Introduction

The attention on the distributed power generation with nuclear energy is increasing due to the electricity grid decentralization and demand for mobile power generation without emission of CO_2. A concept of fully modularized fast reactor with a supercritical CO_2 (S-CO_2) cooled direct Brayton cycle, namely KAIST Micro Modular Reactor (MMR), for 10 MWe power output is being developed for the distributed power generation with the nuclear energy. Furthermore, MMR can be applied to marine propulsion. This is to substitute a diesel engine to meet newly released International Maritime Organization (IMO) regulation on greenhouse gas emission [1].

In the proposed MMR, an appropriate bearing technology to levitate the shaft in the turbomachinery is required. It should be hermetic so that lubrication fluid is not necessary because it forces to add oil supply and sealing sub-system [2, 3]. Since gas bearing does not have enough load to support MMR turbomachinery shaft, magnetic bearing is a proper choice as supported by the previous research [4].

However, an instability issue with magnetic bearing levitation was repeatedly mentioned under S-CO_2 high speed operating conditions. Due to this instability, the shaft eccentricity can grow until the clearance disappears leading to rotor and stator contact. On the other hand, much higher speed operating in air condition does not have the same issue [5].

In former study, the S-CO_2 lubrication pressure distribution in the radial magnetic bearing geometry under uniform circular motion was analyzed. To verify the model results, the shaft trajectory data from the experiments was compared.

In this study, to understand various forces measured from the experiments, the data is further analyzed with Fast Fourier Transform (FFT) method and 2nd order fitting. The instability is discussed in terms of the state space and force distribution.

2. Methods and Results

2.1 Description of Fluid Force in S-CO_2 condition

An Active-control Magnetic Bearing (AMB) levitates a rotating shaft with electromagnets with magnetic force. The force from an electromagnet is expressed as in eq. (1). The AMB's 8 electromagnets are located as shown in Fig. 1. The empty space in Fig. 1 is filled with the working fluid. The fluid can generate vortices and it can destabilize the shaft.

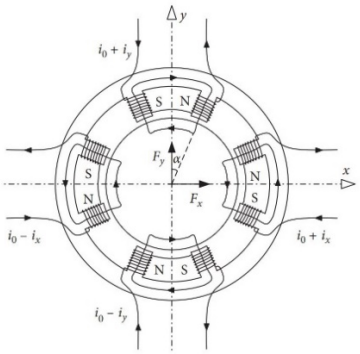

Fig. 1. Electromagnets in the magnetic bearing [6]

$$f = \frac{B^2 A_g}{2\mu_0} = \frac{\mu^2 N^2 I^2 A_g}{2\mu_0 l_g^2} \quad (1)$$

The fluid force is caused by pressure distribution around the shaft. From the former research, this distribution when the shaft center has uniform circular motion is analyzed by using Reynolds equation and Ng-Pan Turbulence model with constant k_x (2) [7, 8]. The geometry where this equation is applied numerically is described in Fig. 2. The analyzed range is summarized in Table I. The fluid force for various thermal properties is shown in Fig 3 and 4.

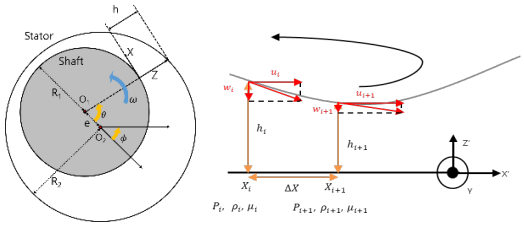

Fig. 2. Coordinate (left) and node (right) description of the unbalanced shaft and the stator

$$\frac{\partial}{\partial X}\left(\frac{\rho h^3}{k_x \mu}\frac{\partial p}{\partial X}\right) = \left(\frac{hu}{2}\right)\frac{\partial \rho}{\partial X} + \left(\frac{u}{2}\frac{\partial h}{\partial X}\right)\rho + \frac{\partial(\rho h)}{\partial t} \quad (2), [7]$$

($k_x = 12 + 0.0388\, Re^{0.8}$, Re : Reynolds number, [8])

Table I. Operation condition range of the model

Supply temperature	20 ~ 50 °C
Supply pressure	70 ~ 100bar
Rotational speed	30000 RPM
Eccentricity ratio, $\varepsilon = e/(R_2 - R_1)$	0.07

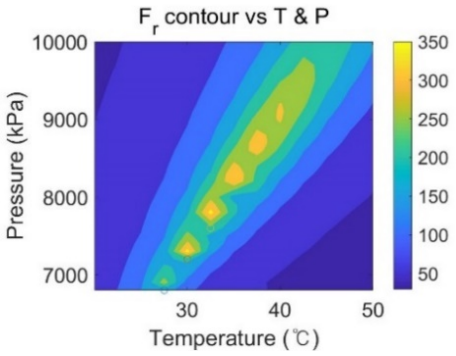

Fig. 3. $\boldsymbol{F_r}$ contour, 30000RPM, ε=0.07

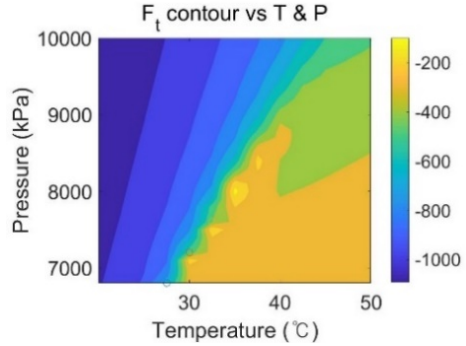

Fig. 4. $\boldsymbol{F_t}$ contour, 30000RPM, ε=0.07

Those contours shows that the lubrication performance has high sensitivity to the fluid conditions. This is more clearly shown from the results of air condition. The significant difference between the S-CO_2 condition and high density air is the spatial density change as shown in Fig 5. The forces of both conditions are summarized in Table II.

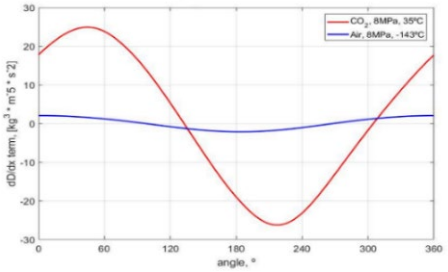

Fig. 5. $\left(\frac{\boldsymbol{hu}}{\mathbf{2}}\right)\frac{\boldsymbol{\partial \rho}}{\boldsymbol{\partial X}}$ around the shaft, $\boldsymbol{\varepsilon}$ = 0.25 and 30,000 RPM

Table II. Force on the shaft, $\boldsymbol{\varepsilon}$ = 0.25 and 30,000 RPM

Thermal condition	F_x (N)	F_z (N)
Air at 8 MPa, -143 ℃	35.3	-1433.6
CO_2 at 8 MPa, 35 ℃	265.2	-1344.7

2.2 Experimental analysis of magnetic bearing instability

From the lubrication model results, it is concluded that the fluid conditions affect the lubrication performance, especially the density change. Therefore, during the experiment, the CO_2's thermal state is controlled by S-CO_2 pressurizing experiment (S-CO_2PE) facility. The AMB test rig consists of the compressor and the AMB. The impeller is removed so only the bearing effect is expected to be dominant.

The tests were proceeded with 8 MPa & 36 ℃ (350kg/m^3) conditions. The one shaft trajectory is shown in Fig. 6. It is observed that the shaft motion does not keep single revolving center when the RPM increases.

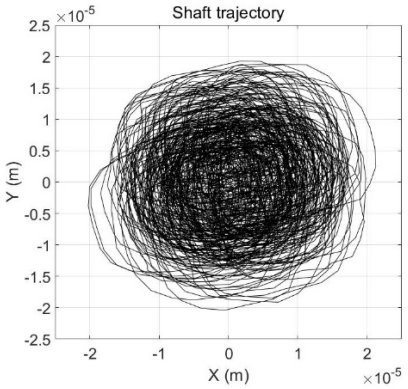

Fig. 6. Shaft trajectory data from S-CO_2 test and 30,000 RPM

The difference of the shaft trajectory from air test and S-CO_2 test is analyzed with Fast Fourier Transform (FFT). The FFT waterfall plot is shown in Fig. 7 for air test and Fig. 8 for S-CO_2 test.

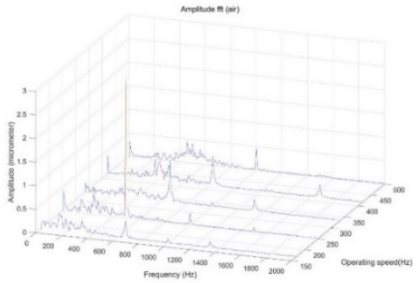

Fig. 7. FFT of the shaft trajectory data from air test

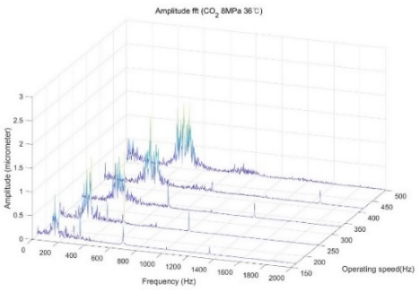

Fig. 8. FFT of the shaft trajectory data from S-CO_2 test

The difference of FFT between air and S-CO_2 test is significant in frequency range lower than operation speed. The noise in this range grows when the fluid whirl appears. To analyze the S-CO_2 effect, fluid force from experiments is calculated.

From this relationship, the stiffness is estimated to be 6.47 N/ μm . However, F_{LUB} does not have strong correlation with ε . To explain this, the correlation between F_{LUB} and the electromagnets' array is analyzed

as shown in Figs. 9 and 10. F_{LUB} in these figures have a period same as electromagnets' array.

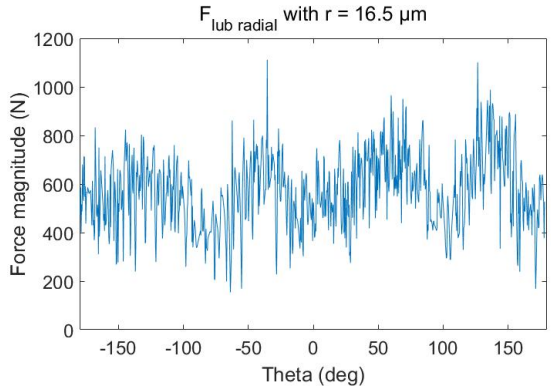

Fig. 9. $F_{LUB,rad}$'s distribution with angular position

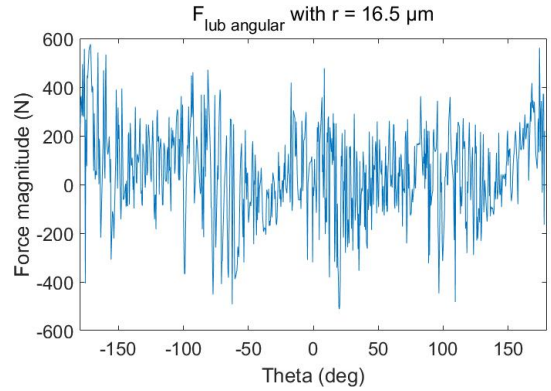

Fig. 10. $F_{LUB,ang}$'s distribution with angular position

Also, the damping in F_{LUB} is obtained. For this goal, the net force is fitted with shaft position and velocity as shown in Fig. 11 and eqs. (3) to (5) [9].

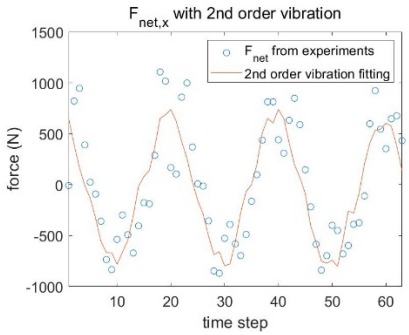

Fig. 11. 2nd order system fitting of the $F_{net,x}$

$$\dot{X} = AX + Bu \tag{3}$$

$$X = \begin{pmatrix} \dot{x} \\ \dot{y} \\ x \\ y \end{pmatrix} \tag{4}$$

$$A = \begin{pmatrix} -\frac{C_{xx}}{m} & -\frac{C_{xy}}{m} & -\frac{K_{xx}}{m} & -\frac{K_{xy}}{m} \\ -\frac{C_{yx}}{m} & -\frac{C_{yy}}{m} & -\frac{K_{yx}}{m} & -\frac{K_{yy}}{m} \\ 1 & 0 & 0 & 0 \\ 0 & 1 & 0 & 0 \end{pmatrix} \tag{5}$$

From Fig. 18, It is shown that the 2nd order system can explain the relationship between the shaft net force and the shaft trajectory. This 2nd order system fitting is planned to be analyzed with control theory in the future.

3. Summary and Conclusions

From the developed lubrication model, it is concluded that the instability of the AMB control can be caused by S-CO_2's physical properties. Tests for various RPMs were performed for verifying the model and the instability sources. The comparison between the model and the tests shows that the spatial change of the fluid density could cause the instability.

The test results with shaft trajectory is analyzed in frequency domain and the forces exerted to the shaft is obtained and compared with model results. This shows significant difference between air and S-CO_2 conditions. In addition, the F_{LUB} is influenced by electromagnets. Obtained forces are considered as a 2nd order vibration system. This system is planned to be analyzed with control theory in the near future. Furthermore, the magnetic bearing's stiffness and damping coefficient will be analyzed for the transient model development. With this, dynamics of the shaft can be established for several different conditions. Well validated model can be adapted to MMR with transient operation. After developing an accurate model, the control logic of the magnetic bearing can be finally suggested.

REFERENCES

[1] Kim, S.G., et al., A concept design of supercritical CO2 cooled SMR operating at isolated microgrid region. International Journal of Energy Research, 2017. 41(4): p. 512-525.
[2] Tsuji, T., et al. Solubility and Liquid Density Measurement for CO2+ Lubricant at High Pressures. in Asian Pacific Confederation of Chemical Engineering congress program and abstracts Asian Pacific Confederation of Chemical Engineers congress program and abstracts. 2004. The Society of Chemical Engineers, Japan.
[3] Seeton, C.J. and P. Hrnjak, Thermophysical properties of CO2-lubricant mixtures and their affect on 2-phase flow in small channels (less than 1mm). 2006.
[4] Sienicki, J.J., et al. Scale dependencies of supercritical carbon dioxide Brayton cycle technologies and the optimal size for a next-step supercritical CO2 cycle demonstration. in SCO2 power cycle symposium. 2011.
[5] Kim, D., S. Baik, and J.I. Lee, Frequency Analysis of Magnetic Journal Bearing Instability for MMR Condition. 2020.
[6] Liu, Y., et al., Research on automatic balance control of active magnetic bearing-rigid rotor system. Shock and Vibration, 2019. 2019.
[7] Hamrock, B.J., B.J. Schmid, and B.O. Jacobson, Fundamentals of fluid film lubrication. Vol. 169. 2004: CRC press.
[8] Taylor, C. and D. Dowson, Turbulent lubrication theory—application to design. 1974.
[9] Li, Q., et al., Active rotordynamic stability control by use of a combined active magnetic bearing and hole pattern seal component for back-to-back centrifugal compressors. Mechanism and Machine Theory, 2018. 127: p. 1-12.